Nano Research

Open Access

Research Article

High-quality boron nitride nanosheets via polymer anchoring and thin-layer confined shearing exfoliation

Yiqing Zhou, Zetong Zhuang, Jiaojiao Feng, Haonan Xiong, and Chun Li ✉

Key Lab of Organic Optoelectronics and Molecular Engineering of Ministry of Education, Laboratory of Flexible Electronics Technology, Department of Chemistry, Tsinghua University, Beijing 100084, China

Cite this article: *Nano Research*, **2026**, *19*, 94908319. https://doi.org/10.26599/NR.2026.94908319

ABSTRACT: Flexible, lightweight, and electrically insulated materials with high thermal conductivity and good mechanical performance are highly required for next-generation electronic devices. Hexagonal boron nitride nanosheet (BNNS) has a great potential to meet these requirements because of its high thermal conductivity, intrinsic insulation, and superior stability. However, the production of solution-processing, high quality BNNSs with larger lateral size is still challenged. Herein, we develop a thin-layer confined shearing and polymer-anchoring strategy for the exfoliation of hexagonal boron nitride (h-BN) into BNNSs. Upon optimization of the rotation speed of milling tools, chemical structure of anchored polymer, the layer thickness and rheological properties of liquid medium, the shearing force applied on h-BN crystals increases greatly. The anchored polymer (sodium carboxymethyl cellulose, CMC) can effectively promote shearing force transfer and impact buffer onto the h-BN crystals, consequently improving the exfoliation yield (84.6%) and giving BNNSs with large lateral size (1.97 ± 1.09 μm) and high aspect ratio (~ 746). The anchored polymer endows BNNSs with good hydrophilicity and solution processability. The BNNS (78 wt.%)/CMC film prepared by spatially confined evaporation has densely packed structure, exhibiting high tensile strength (289 ± 21 MPa) and high in-plane thermal conductivity (59.5 ± 2.7 W·m^{-1}·K^{-1}). Electrically-insulating yet highly thermally conducting nature enables BNNS films attractive in insulated thermal management applications.

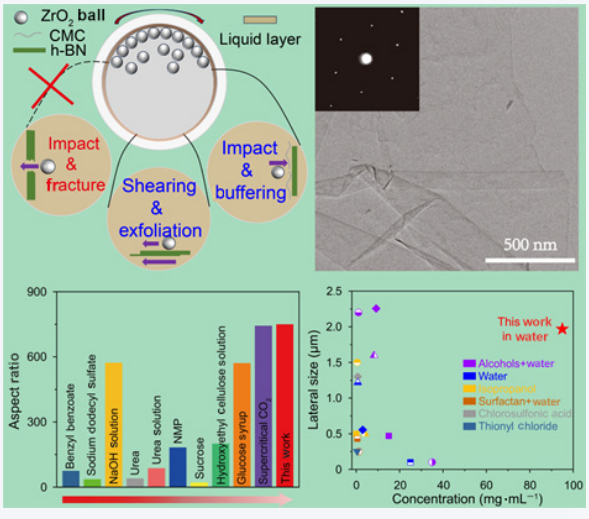

KEYWORDS: boron nitride nanosheets, water-dispersible, thin-layer confined shearing, polymer-anchoring, flexible films, thermal conductivity

1 Introduction

With the rapid development of miniaturized, highly integrated electronic devices, advanced thermal management materials (TMMs) have attracted ever-increasing attention since effective heat conduction and heat dissipation are vitally important to the performance and reliability of high-power electronics [1–3]. Among TMMs, two-dimensional (2D) hexagonal boron nitride nanosheet (BNNS) exhibits unique advantages including high intrinsic thermal conductivity, excellent electrical insulation, low thermal expansion coefficient, mechanical flexibility, and superior chemical, environmental, and thermal stability [3–7]. Electrically-insulating yet thermally conducting nature enables BNNS and its composites very ideal TMMs in electronics, electrical packaging, and thermal conductive coating, significantly decreasing the risk of signal interference and short-circuits [8–11].

Despite having extraordinary performance as TMMs, its device applications are still greatly limited due to the lack of cost-effective routes towards mass production of high-quality BNNSs with large lateral size, high aspect ratio, and good processability [6, 12, 13]. Top-down planetary ball milling exfoliation has been widely applied to prepare 2D BNNSs from hexagonal boron nitride (h-BN) crystals, by which shear force is utilized to overcome the interactions between h-BN layers (Van Der Waals force) [4, 6, 14–19]. However, due to the strong interaction between h-BN

Received: September 24, 2025; **Revised:** November 12, 2025
Accepted: December 8, 2025

✉Address correspondence to chunli@mail.tsinghua.edu.cn

layers, the exfoliation energy of bulk h-BN is much higher than that of graphite [20]. To maximize the amount of energy transferred from milling tools to h-BN crystals, high rotational speed of the pots and disk was generally used to enlarge shear and impact energies of milling balls inside the pots [6]. Unfortunately, the large impact forces usually give small and thick BNNSs [6, 19]. Reducing the rotation speed can effectively decrease the impact energy, but at the cost of shear energy and exfoliation efficiency. Thus, the strategies that can increase the shear energy and lower the impact energy simultaneously are highly desirable for ball milling exfoliation of h-BN crystals. For instance, a viscous solvent-assisted planetary ball milling method has been developed to produce large and thin BNNSs with a high exfoliation yield of 74% [19].

Being sharply contrast to graphene, BNNSs are more difficult to be functionalized due to its high chemical inertness [6]. Generally, small amount of functional group can be grafted to the edge/in-plane sites of BNNSs during ball milling exfoliation process or by post-functionalization, thus giving BNNS colloid dispersions with relatively low concentrations (with an order of 0.1–2.0 mg·mL^{-1}) [6], limiting its processibility and applications. Although great progress has been achieved in the preparation, processing, and applications of BNNSs, the scalable preparation of functionalized BNNSs with large lateral size and good dispersibility is still challenged [6, 12, 13].

In this work, we develop a thin-layer confined shearing and polymer-anchoring strategy for the scalable exfoliation of h-BN crystals into BNNSs. Upon optimization of the rotation speed of the ball milling tools, chemical structure of anchored polymer, and the layer thickness and rheological properties of the liquid medium, the shearing force applied onto h-BN crystals increases greatly. Simultaneously, the anchored polymer can effectively buffer the impact force onto the h-BN crystals. Consequently, the developed method can greatly improve the exfoliation yield (84.6%) and give BNNSs with large lateral size (1.97 ± 1.09 μm) and high aspect ratio (~ 746). The anchored polymer endows the BNNSs with good hydrophilicity and solution processability. The BNNS composites films prepared by spatially confined evaporation has densely packed structure (1.96 g·cm^{-3}), exhibiting high tensile strength (289 ± 21 MPa) and high in-plane thermal conductivity (59.5 ± 2.7 W·m^{-1}·K^{-1}), making them attractive in insulated thermal management applications.

2 Results and discussion

Mechanical exfoliation and pulverization of h-BN crystals in planetary ball mills are complex and mainly dependent on the rotation speed, milling time, the size and quantity of the mill balls, filling ratio of milling balls to the samples (at constant chamber size) as well as the choice of an appropriate liquid medium [6, 21]. High rotation speed generally increases the energy input and promotes the exfoliation of h-BN crystals, but can also induce strong collisions and vertical impacts to fracture h-BN crystals and destroy crystallinity (Fig. 1(a)) [6, 19, 21]. Therefore, relatively low rotation speed and viscous medium can help in lowering the energy of collision, favoring the preparation of large and high-quality BNNSs [6, 19].

In addition to buffering the impact force, liquid medium with high viscosity can greatly increase shear force. Although the exact exfoliation process could be far more complex, under the shear force-dominated milling process with an appropriate quantity of mill balls and relatively low rotation speed (250 rpm), shear stress of the liquid medium can be semi-quantitatively evaluated based on a steady-state assumption (Fig. 1(b)) [21], in which the interface slip between the viscous medium and the tank sidewall is neglectable.

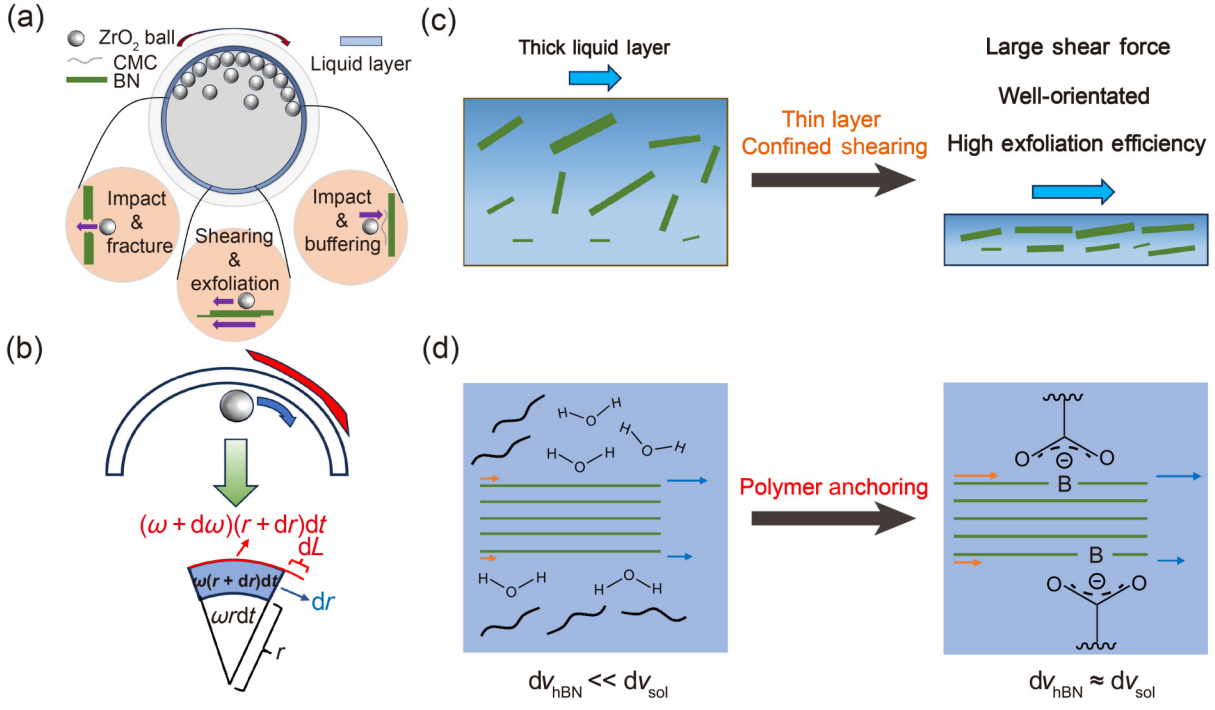

Figure 1 Schematic illustration of thin-layer confined shearing and polymer-anchoring strategy for the exfoliation of h-BN crystals. (a) Illustration of shearing and impact force on the h-BN crystals. (b) Simplified model for analyzing shear force. Arrows represent the motion direction and relative speed of ball-milling tank (red) and ball-milling beads (blue). (c) Mechanism of thin-layer confined shearing. Blue arrows represent the direction and magnitude of shear force. (d) Polymer-anchoring on the h-BN surface.

The shear rate ($\dot{\gamma}$) and shear force (τ) of viscous liquid layer can be described as $\tau = \eta \cdot \dot{\gamma} = \eta \frac{dv}{dr}$, where η is the viscosity of liquid medium, dv is the relative velocity between milling ball and tank sidewall, and dr is the liquid layer thickness. Obviously, under the identical rotation speed and medium, the thinner the liquid layer, the higher the shear force (Fig. 1(c)).

To enhance shear force transfer between the liquid medium and the layered h-BN crystals, aqueous sodium carboxymethyl cellulose (CMC) solution was used as the liquid medium due to its high viscosity and potential anchoring ability towards h-BN surface (similar to Lewis bases amine molecules [22]) (Fig. 1(d)). It is expected that thin-layer confined shearing in a medium with high viscosity, combining with the polymer-anchored strategy would greatly increase shear force and thus achieve high exfoliation efficiency, as verified by following experimental results.

Aqueous CMC-functionalized BNNS dispersion, with a high exfoliation yield (up to 84.6%) was readily prepared by thin-layer confined shearing h-BN crystals in an aqueous CMC dispersion with high viscosity (Fig. S1 and Tables S1–S4 in the Electronic Supplementary Material (ESM)). For clarity, the abbreviation "BNNS-x" was utilized to designate the CMC-functionalized BNNS, where x signifies the mass fraction (wt.%) of BNNS in the composite and is dependent on the feeding mass ratio of h-BN to CMC (Fig. S1 and Table S5 in the ESM). Typically, the rotation and revolution speeds of planetary ball mills were set at 250 and 125 rpm, respectively, being characteristic of low speeds and less energy input [14–19]. ZrO_2 balls with diameters of 10 mm (150 g) and 2.22 mm (30 g), and 6.5 g aqueous CMC (1.8 wt.%) solution containing 0.86 g h-BN crystals (Fig. S2 in the ESM) were loaded into a 500 mL ZrO_2 pot to give a thin liquid layer with a thickness of ~ 220 μm and ball-to-powder ratio of 209. After 20 h grinding, followed by a mild sonication and further centrifugation, aqueous BNNS dispersion with a milky white color and obvious Tyndall effect was obtained (Fig. 2(a)), indicating the formation of CMC-functionalized BNNS (BNNS-86) colloid with good dispersibility (Fig. 2(b), up to 95 mg·mL^{-1}, being the highest reported) [15–19, 23–34]. More impressively, the dispersion (5 mg·mL^{-1}) is uniform and very stable, and no obvious stratification or precipitation was observed even after 30 days of storage (Fig. S3 in the ESM).

In X-ray diffraction (XRD) patterns (Fig. S4 in the ESM), the broader and weaker (002) peak of BNNSs relative to h-BN crystals further confirms the decreased thickness and smaller crystal size of BNNS caused by the exfoliation [17]. It has also been demonstrated that the proposed strategy can be readily applied for the exfoliation of h-BN crystals in organic solvent and other 2D materials (Fig. S5 in the ESM).

BNNSs had an average lateral size of 1.97 ± 1.09 μm and a thickness of 2.46 ± 1.3 nm (Figs. 2(c)–2(e) and Fig. S6 in the ESM), giving an aspect ratio of 746, which is among the highest reported

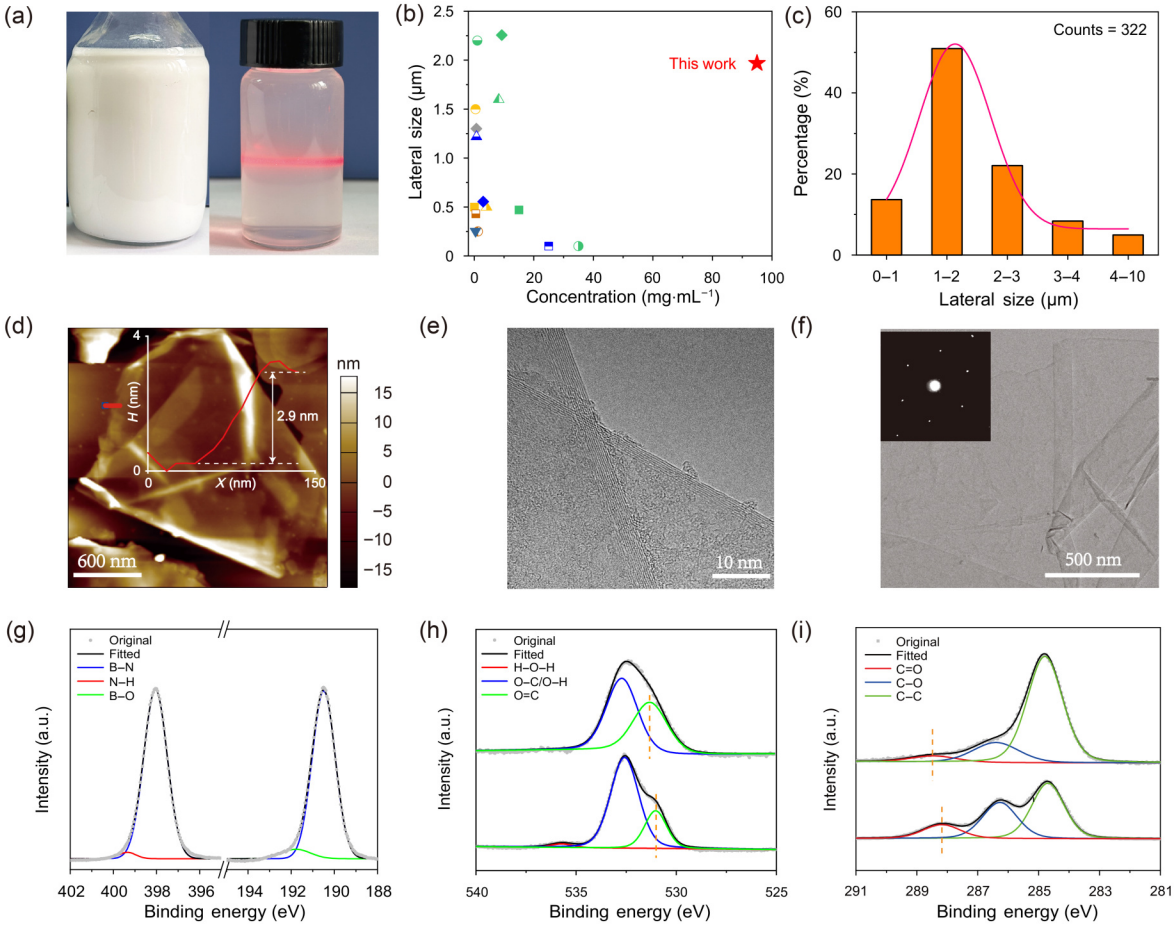

Figure 2 Characterization of aqueous BNNS-86 dispersion and BNNS-86. (a) Photograph of as-prepared BNNS-86 dispersion (5 mg·mL^{-1}) and Tyndall effect of dilute BNNS-86 dispersion (0.04 mg·mL^{-1}). (b) Comparison of concentration and lateral size of BNNS-86 with those reported previously. Original data are listed in Table S6 in the ESM. (c) Statistical analysis of the lateral size from SEM. (d) Typical AFM image. (e) HRTEM image of curved BNNS-86. f) TEM image and SAED pattern (inset). (g) N 1s (left) and B 1s (right) XPS patterns of BNNS-86. (h) O 1s and (i) C 1s XPS patterns of BNNS-86 (top) and CMC (bottom).

(Table S7 in the ESM) [14–19, 31–36]. The lateral size was evaluated based on the statistical analysis of scanning electron microscopy (SEM) images of BNNSs, being consistent with the results of dynamic light scattering measurement (Fig. S6 in the ESM). To eliminate the influence of CMC anchored on BNNSs, the average thickness of BNNSs was measured via high resolution transmission electron microscopy (HRTEM) (Fig. 2(e) and Fig. S7 in the ESM). The wrinkles and folded/curled structures observed in AFM and TEM images of BNNSs signify good mechanical flexibility of BNNSs originated from the ultrathin feature with few layers (Figs. 2(d)–2(f)). A typical six-fold symmetry selected area electron diffraction (SAED) pattern shown in the inset of Fig. 2(f) demonstrates that the intact hexagonal lattice of BNNS is well preserved after exfoliation. X-ray photoelectron spectroscopy (XPS) patterns of B 1s and N 1s electrons (Fig. 2(g)) reveal that there are few B–O (191.8 eV) and N–H (398.3 eV) groups grafted to the BNNSs as the pristine h-BN crystals (Fig. S2 in the ESM) [17, 37], demonstrating a low degree of defects and covalent functionalization under relatively lower rotation speeds with less energy input.

Anchored polymer facilitates the exfoliation of h-BN crystals and plays an important role on the water dispersibility of the resultant BNNSs. As shown in Figs. 2(h) and 2(i), the binding energies of carbonyl O 1s (531.32 eV) and C 1s (288.46 eV) electrons of CMC-functionalized BNNSs exhibit noticeable up-shifts with respect to those of CMC (531.01 and 288.17 eV) [38], indicating the presence of electron transfer originated from strong interaction between CMC and BNNSs. It was proposed that, with the assistance of energy input during ball milling, carboxylate moieties of CMC can interact with boron atoms on the surface of h-BN crystals via non-covalent interaction [22]. Consequently, the anchored CMC greatly promotes the shearing force transfer and the exfoliation of h-BN crystals into ultrathin BNNSs in high yield [39]. It is worth noting that polymer anchoring and exfoliation of h-BN crystals is strongly influenced by the chemical structure of polymer. For instance, under the identical exfoliation condition (Fig. S8 in the ESM), employing sodium alginate (SA), an analogue of CMC, as the viscous medium results in a poor exfoliation efficiency, giving BNNSs with large thickness and poor stability in aqueous dispersion (Fig. S9 in the ESM). This difference would be originated from the high steric hindrance of carboxylic groups in SA, limiting its interaction with h-BN crystals (Fig. S9 in the ESM).

Force-induced CMC-functionalized BNNSs create a superior hydrophilic structure, as confirmed by the contact angle and zeta potential measurements. The non-covalent functionalization of basal plane render BNNSs more hydrophilic, with a water contact angle of 26.0° (BNNS-86, Fig. S10 in the ESM), being much smaller than those of pristine BNNS (87°) [40], and BNNSs with hydroxyl (BNNS-OH, 59.9°) [33] or amino groups (BNNS-NH_2, 43° ± 1°) [17] bonded to the edges and defect sites. The zeta potential of BNNS-86 in water was estimated to be −45.3 ± 1.3 mV, which is more negative than those of glucose-g-BNNS (−36.7 mV) [18] and BNNS-NH_2 (−34 ± 4 mV) [17]. The surface anchored structure of CMC-functionalized BNNSs is believed to account for its better hydrophilicity relative to BNNSs with hydrophilic groups bonded to the edges and defect sites, due to the blocking of hydrophobic basal plane of BNNSs by the surface-anchored CMC. The anchored CMC prevents re-agglomeration of BNNSs, giving stable BNNS colloid solutions with excellent processibility (Fig. 2(b)).

CMC-functionalized BNNSs can be readily processed into highly orientated, densely packed films with superior mechanical and thermal performance via vacuum-assisted filtration (f-BNNS-*x*) or spatially confined evaporation [41] (e-BNNS-*x*). Both e-BNNS and f-BNNS films can be readily peeled off from the substrate membranes, giving free-standing paper-like films with laminated structure and homogeneous distribution of C, O, B and N elements within film matrix (Figs. 3(a)–3(c)). These films are smooth, foldable, and can be easily processed into the desired shapes (Fig. S11 in the ESM). The thicknesses and sizes can be easily adjusted by the feeding amounts of BNNS dispersion and the sizes of substrates, especially for the e-BNNS films by spatially confined evaporation. As shown in Fig. 3(d), all XRD patterns of BNNS-*x* films exhibit a sharp diffraction peak, demonstrating the formation of a highly orientated laminated structure [41]. With increasing the amount of CMC, the diffraction peak of BNNS-86 film (2θ = 26.82°) was shifted to a smaller angle (2θ = 26.66°) for BNNS-71 film, signifying the slight enlargement of the interlayer distances between BNNSs. In combination with the homogeneous distribution of C, O, B and N elements across the fracture surfaces of the films recorded by energy dispersive spectroscopy (EDS) mappings (Fig. 3(c)), it is reasonable to conclude that CMC has been anchored on the BNNS surface and homogeneously intercalated into BNNS interlayers without phase separation. Further increasing CMC content, the diffraction peak of BNNS-71 film remains the same as BNNS-78 film, suggesting that the amount of anchored CMC has become saturated and aggregation of CMC has appeared.

As shown in Fig. 3(e), the tensile strength and toughness of BNNS films are strongly dependent on the composition and processing methods. With increasing the content of CMC (15 wt.%–30 wt.%), the BNNS films become stronger and tougher irrespective of the processing methods. The tensile stress of e-BNNS-86 films was measured to be 224 ± 21 MPa with a strain of 0.57% ± 0.06% (Fig. 3(e)), which is 1.9 times that of the f-BNNS-86 films (118 ± 14 MPa). The mechanical properties of BNNS composite films can be further improved by increasing CMC component. The e-BNNS-71 films exhibit the highest tensile strength of 305 ± 24 MPa with a strain of 1.55% ± 0.09% and the modulus of 47.2 ± 6.1 GPa. The volumetric toughness of e-BNNS-71 films was calculated to be 3.54 ± 0.23 $MJ{\cdot}m^{-3}$ by integrating the areas under the stress–strain curves. To the best of our knowledge, these values are the highest among the reported BNNS-based film materials [9, 18, 29, 30, 33, 39, 42–61] (Figs. 3(f) and 3(g), and Tables S8 and S9 in the ESM).

The large lateral size, superior hydrophilicity and ultrathin feature of CMC-functionalized BNNSs synergistically contribute to the impressive mechanical performance. It is known that for the solution processing 2D materials films, the capillary force (P_c) plays an important role on the densification of the films, and can be expressed as $P_c = -\frac{2\gamma\cos\theta}{r}$ [62], where γ is the surface tension of solution, θ is the contact angle of CMC-anchored BNNS, and r is the pore radius of voids within the film matrix. Obviously, hydrophilic CMC-anchored BNNS with smaller water contact angle is favorable for the increase of capillary force to densify the resultant BNNS films. Simultaneously, the ultrathin feature enables CMC-anchored BNNS have a lower bending rigidity, intending to bend and buckle under the capillary force, removing the voids within the film matrix, and finally giving compact and highly orientated films [41]. With increasing CMC content, the CMC-functionalized BNNS becomes more hydrophilic (Fig. S10 in the ESM), which is favorable for enhancing capillary force within the

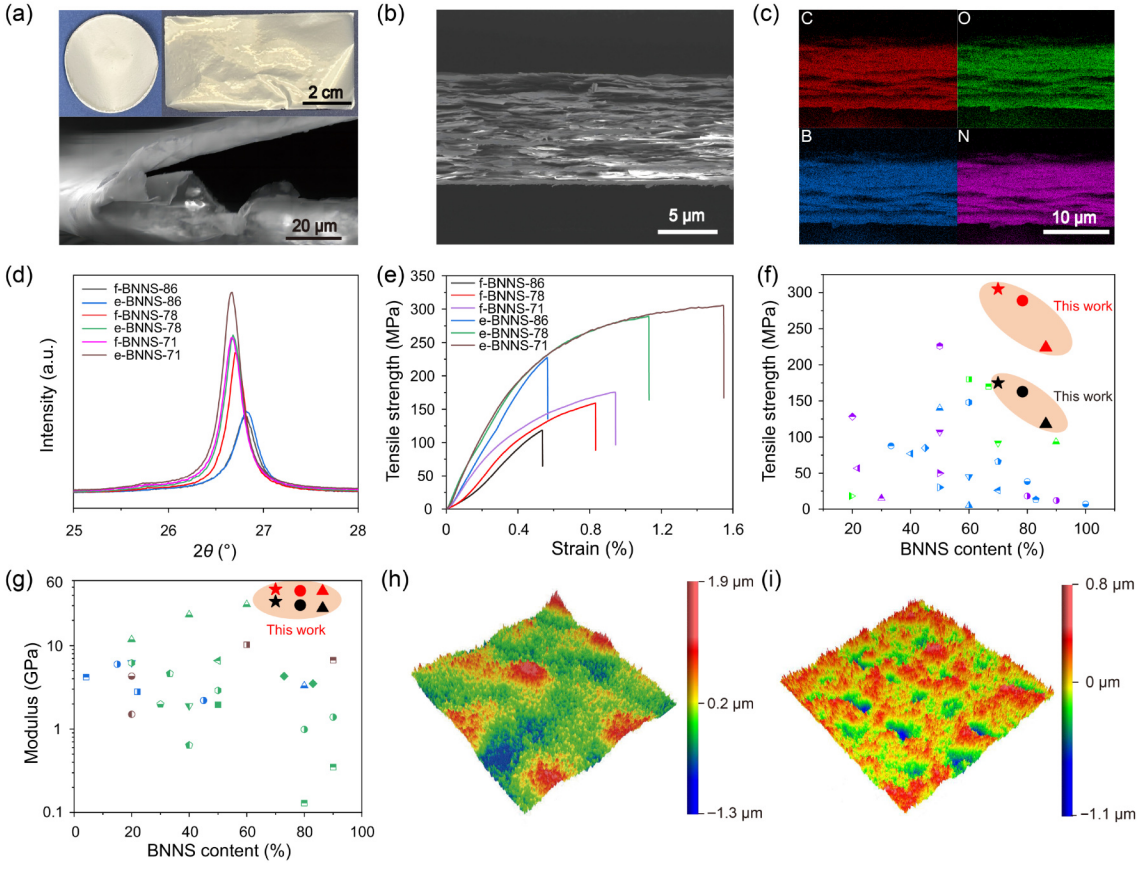

Figure 3 Characterizations of the BNNS films. (a) Photographs of BNNS films by different processing methods (top) and SEM image of the cross section of a folded e-BNNS-78 film (bottom). (b) SEM image of the cross section of e-BNNS-78 film and (c) corresponding EDS mappings. (d) XRD patterns of BNNS films as indicated. (e) Typical stress-strain curves of BNNS films as indicated. Comparison of (f) the tensile strength and (g) modulus of BNNS-*x* films (red for e-BNNS-*x* and black for f-BNNS-*x*; Star: BNNS-71; Square: BNNS-78; Up rectangle: BNNS-86) with those reported previously. Original data are shown in Tables S8 and S9 in the ESM. Top surface height profile images of (h) f-BNNS-86 and (i) e-BNNS-86 films taken by optical profilometry with a view field of 834 μm × 834 μm.

film matrix, and thus facilitating the formation of more compact BNNS films with improved alignment and fewer defects (microvoids) as evidenced by the increase in (002) peak intensity (Fig. 3(d)) and the improved packing density (Fig. S12 in the ESM). Consequently, the mechanical properties of the resultant films are significantly improved (Figs. 3(e)–3(g) and Fig. S12 in the ESM).

The mechanical property of BNNS films depends strongly on the film microstructures induced by the processing processes. The surface morphology of the BNNS-86 films was inspected by optical profilometry (Figs. 3(h) and 3(i)) and SEM (Fig. S13 in the ESM). The e-BNNS-86 film by spatially confined evaporation exhibited smaller surface protrusions with respect to the f-BNNS-86 film via vacuum-assisted filtration, and the root mean square (RMS) roughness of the film surfaces decreased significantly from 364 nm for f-BNNS-86 to 198 nm for e-BNNS-86. It is believed that during spatially confined evaporation, the shear stress and surface anchoring effect promoted BNNS alignment in the dispersion, and ultrathin BNNSs with large lateral size tend to bend and buckle, and finally form a densely packed e-BNNS films with less defects (voids) and superior mechanical performance, as reported previously [41].

Large lateral size of the building block BNNS and densely packed structure of BNNS films endow the films with extraordinary high thermal conductivity (Fig. S14 in the ESM). The e-BNNS-78 film with an apparent packing density of 1.96 g·cm^{-3} exhibits a highest in-plane thermal conductivity of 59.5 ± 2.7 W·m^{-1}·K^{-1} (Fig. 4(a) and Fig. S15 in the ESM), being among the highest reported [9, 18, 19, 29, 30, 33, 34, 39, 42, 46–52, 54, 57–61, 63–66]. The integration of light weight, high strength, high toughness, excellent electrical insulation, and high thermal conductivity enable the BNNS films have great potentials as flexible and insulated TMMs. Being different from the widely used conductive graphite films, insulated e-BNNS-78 film exhibits excellent transmission performance with electromagnetic interference (EMI) shielding effectiveness (SE) of 2 mdB in X-band (Fig. 4(b)). The performance of e-BNNS-78 film (15 μm) as planar heat dissipation material was evaluated by the model device as depicted in Fig. 4(c). It can be seen that the central temperature of e-BNNS-78 film is 17 °C higher than that of the control CMC film after 270 s (Figs. 4(c) and 4(d)), revealing the excellent flat heat dissipation capacity of e-BNNS-78 film. To evaluate the cooling efficiency of the BNNS films as a thermal interface material (TIM), e-BNNS-78 film (15 μm) was placed between a LED chip (10 W) and a heat sink (Fig. S16 in the ESM). As shown in Fig. 4(e), compared to the case without BNNS film as TIM, the central temperature of the top surface of LED chip can decrease by 9 °C after 70 s, demonstrating good cooling capacity.

3 Conclusions

In summary, we have developed a facile polymer-anchoring and thin-layer confined shearing strategy for the mass production of water-dispersible BNNSs with a large lateral size, high aspect ratio. We demonstrate that rotation speeds (energy input), filling ratio of

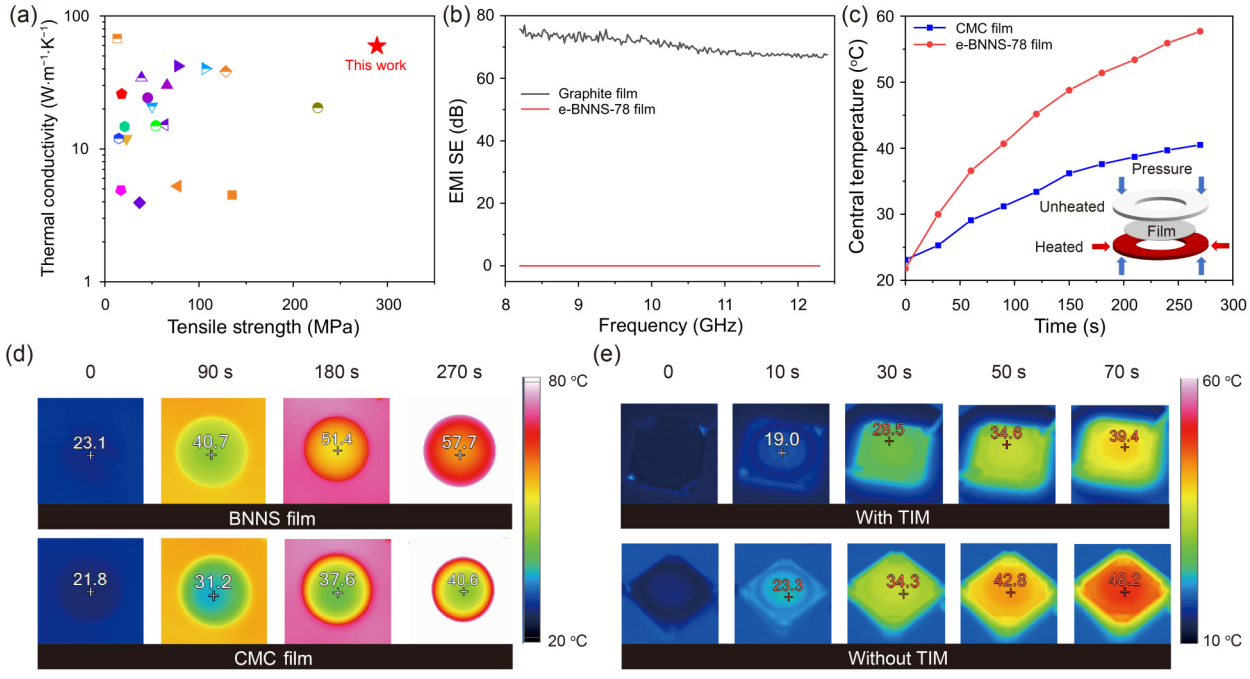

Figure 4 Characterization of the insulated and thermally conductive performance of e-BNNS-78 film. (a) Comparison of thermal conductivity and tensile strength of e-BNNS-78 film with those of BNNS-based films reported previously. Original data are listed in Table S10 in the ESM. (b) EMI shielding effectiveness SE of e-BNNS-78 and graphite films. (c) Temperature evolution of the film center as indicated and the diagram for model device (inset). (d) Infrared thermal images of the e-BNNS-78 and control CMC films recorded at different time. (e) Infrared thermal images of the top surface of LED chip with/without the TIMs as indicated.

milling balls to the samples (liquid layer thickness), chemical structure of anchored polymer as well as viscosity of liquid medium have significant impacts on the exfoliation yield and aspect ratio of BNNSs. The CMC-functionalized BNNSs can be readily processed into free-standing paper-like films by vacuum-assisted filtration or spatially confined evaporation methods. The films with densely packed structure exhibit high tensile strength (289 ± 21 MPa), high modulus, and high in-plane thermal conductivity (59.5 ± 2.7 $W·m^{-1}·K^{-1}$). This work not only provides a simple method for the preparation of high-quality BNNS dispersion and high-performance BNNS-based films but also has wide implications in understanding the exfoliation process of h-BN crystals. The excellent properties, along with high exfoliation yield, ease of mass production and processing, pave the way for practical applications of BNNSs in insulated thermal management applications, especially for how-power communication equipment such as mobile phone, tablet computer, 5G base station, and mini Wi-Fi router.

Electronic Supplementary Material: Supplementary material (SEM images, TEM images, XRD patterns, XPS patterns, etc.) is available in the online version of this article on https://doi.org/10.26599/NR.2026.94908319.

Data availability

All data needed to support the conclusions in the paper are presented in the manuscript and the Electronic Supplementary Material. Additional data related to this paper may be requested from the corresponding author upon request.

Acknowledgements

This work was supported by the National Key Research and Development Program of China (Nos. 2022YFB3804901 and 2022YFB3804900). We gratefully acknowledge the helpful discussions with Mr. Xiaoang Yuan and Dr. Enlai Gao.

Declaration of competing interest

All the contributing authors report no conflict of interests in this work.

Author contribution statement

Y. Q. Z.: Conceptualization, data curation, formal analysis, methodology, investigation, validation, visualization, writing – original draft, writing – review & editing. Z. T. Z.: Software, data curation. J. J. F.: Data curation, investigation. H. N. X.: Formal analysis. C. L.: Project administration, funding acquisition, investigation, supervision, writing – original draft, writing – review & editing. All the author have approved the final manuscript.

Use of AI statement

None.

References

[1] Wang, Z. F.; Wu, Z. J.; Weng, L.; Ge, S. B.; Jiang, D. W.; Huang, M. N.; Mulvihill, D. M.; Chen, Q. G.; Guo, Z. H.; Jazzar, A. et al. A roadmap review of thermally conductive polymer composites: Critical factors, progress, and prospects. *Adv. Funct. Mater.* **2023**, *33*, 2301549.

[2] Lin, Y.; Li, P. L.; Liu, W. J.; Chen, J.; Liu, X. Y.; Jiang, P. K.; Huang, X. Y. Application-driven high-thermal-conductivity polymer nanocomposites. *ACS Nano* **2024**, *18*, 3851–3870.

[3] Dai, W.; Wang, Y. D.; Li, M. H.; Chen, L.; Yan, Q. W.; Yu, J. H.;

Jiang, N.; Lin, C. T. 2D materials-based thermal interface materials: Structure, properties, and applications. *Adv. Mater.* **2024**, *36*, 2311335.

[4] Weng, Q. H.; Wang, X. B.; Wang, X.; Bando, Y.; Golberg, D. Functionalized hexagonal boron nitride nanomaterials: Emerging properties and applications. *Chem. Soc. Rev.* **2016**, *45*, 3989–4012.

[5] Song, H. F.; Liu, J. M.; Liu, B. L.; Wu, J. Q.; Cheng, H. M.; Kang, F. Y. Two-dimensional materials for thermal management applications. *Joule* **2018**, *2*, 442–463.

[6] Roy, S.; Zhang, X.; Puthirath, A. B.; Meiyazhagan, A.; Bhattacharyya, S.; Rahman, M. M.; Babu, G.; Susarla, S.; Saju, S. K.; Tran, M. K. et al. Structure, properties and applications of two-dimensional hexagonal boron nitride. *Adv. Mater.* **2021**, *33*, 2101589.

[7] Bhattacharjee, A.; Jiang, H. B.; Li, L. H.; Huang, S. M.; Chen, Y. I.; Cai, Q. R. Thermal transport property of boron nitride nanosheets. *Appl. Phys. Rev.* **2024**, *11*, 041322.

[8] Chen, J.; Huang, X. Y.; Sun, B.; Jiang, P. K. Highly thermally conductive yet electrically insulating polymer/boron nitride nanosheets nanocomposite films for improved thermal management capability. *ACS Nano* **2019**, *13*, 337–345.

[9] Chen, Y.; Zhang, H. G.; Chen, J.; Guo, Y. T.; Jiang, P. K.; Gao, F.; Bao, H.; Huang, X. Y. Thermally conductive but electrically insulating polybenzazole nanofiber/boron nitride nanosheets nanocomposite paper for heat dissipation of 5G base stations and transformers. *ACS Nano* **2022**, *16*, 14323–14333.

[10] Zhao, C. G.; Li, Y. F.; Liu, Y. C.; Xie, H. Q.; Yu, W. A critical review of the preparation strategies of thermally conductive and electrically insulating polymeric materials and their applications in heat dissipation of electronic devices. *Adv. Compos. Hybrid Mater.* **2023**, *6*, 27.

[11] Chen, Q. G.; Yang, K. L.; Feng, Y.; Liang, L.; Chi, M. H.; Zhang, Z. H.; Chen, X. S. Recent advances in thermal-conductive insulating polymer composites with various fillers. *Compos. Part A: Appl. Sci. Manuf.* **2024**, *178*, 107998.

[12] Martínez-Jiménez, C.; Chow, A.; Smith McWilliams, A. D.; Martí, A. A. Hexagonal boron nitride exfoliation and dispersion. *Nanoscale* **2023**, *15*, 16836–16873.

[13] An, L. L.; Yu, Y. L.; Cai, Q. R.; Mateti, S.; Li, L. H.; Chen, Y. I. Hexagonal boron nitride nanosheets: Preparation, heat transport property and application as thermally conductive fillers. *Prog. Mater. Sci.* **2023**, *138*, 101154.

[14] Li, L. H.; Chen, Y.; Behan, G.; Zhang, H. Z.; Petravic, M.; Glushenkov, A. M. Large-scale mechanical peeling of boron nitridenanosheets by low-energy ball milling. *J. Mater. Chem.* **2011**, *21*, 11862–11866.

[15] Yao, Y. G.; Lin, Z. Y.; Li, Z.; Song, X. J.; Moon, K. S.; Wong, C. P. Large-scale production of two-dimensional nanosheets. *J. Mater. Chem.* **2012**, *22*, 13494–13499.

[16] Lee, D.; Lee, B.; Park, K. H.; Ryu, H. J.; Jeon, S.; Hong, S. H. Scalable exfoliation process for highly soluble boron nitride nanoplatelets by hydroxide-assisted ball milling. *Nano Lett.* **2015**, *15*, 1238–1244.

[17] Lei, W. W.; Mochalin, V. N.; Liu, D.; Qin, S.; Gogotsi, Y.; Chen, Y. Boron nitride colloidal solutions, ultralight aerogels and freestanding membranes through one-step exfoliation and functionalization. *Nat. Commun.* **2015**, *6*, 8849.

[18] Chen, S. H.; Xu, R. Z.; Liu, J. M.; Zou, X. L.; Qiu, L.; Kang, F. Y.; Liu, B. L.; Cheng, H. M. Simultaneous production and functionalization of boron nitride nanosheets by sugar-assisted mechanochemical exfoliation. *Adv. Mater.* **2019**, *31*, 1804810.

[19] Zhou, Y. C.; Xu, L. S.; Liu, M. S.; Qi, Z.; Wang, W. B.; Zhu, J. Y.; Chen, S. H.; Yu, K.; Su, Y.; Ding, B. F. et al. Viscous solvent-assisted planetary ball milling for the scalable production of large ultrathin two-dimensional materials. *ACS Nano* **2022**, *16*, 10179–10187.

[20] Jung, J. H.; Park, C. H.; Ihm, J. A rigorous method of calculating exfoliation energies from first principles. *Nano Lett.* **2018**, *18*, 2759–2765.

[21] Burmeister, C. F.; Kwade, A. Process engineering with planetary ball mills. *Chem. Soc. Rev.* **2013**, *42*, 7660–7667.

[22] Lin, Y.; Williams, T. V.; Connell, J. W. Soluble, exfoliated hexagonal boron nitride nanosheets. *J. Phys. Chem. Lett.* **2010**, *1*, 277–283.

[23] Coleman, J. N.; Lotya, M.; O'Neill, A.; Bergin, S. D.; King, P. J.; Khan, U.; Young, K.; Gaucher, A.; De, S.; Smith, R. J. et al. Two-dimensional nanosheets produced by liquid exfoliation of layered materials. *Science* **2011**, *331*, 568–571.

[24] Smith, R. J.; King, P. J.; Lotya, M.; Wirtz, C.; Khan, U.; De, S.; O'Neill, A.; Duesberg, G. S.; Grunlan, J. C.; Moriarty, G. et al. Large-scale exfoliation of inorganic layered compounds in aqueous surfactant solutions. *Adv. Mater.* **2011**, *23*, 3944–3948.

[25] Morishita, T.; Okamoto, H. Facile exfoliation and noncovalent superacid functionalization of boron nitride nanosheets and their use for highly thermally conductive and electrically insulating polymer nanocomposites. *ACS Appl. Mater. Interfaces* **2016**, *8*, 27064–27073.

[26] Sun, W. L.; Meng, Y.; Fu, Q. R.; Wang, F.; Wang, G. J.; Gao, W. H.; Huang, X. C.; Lu, F. S. High-yield production of boron nitride nanosheets and its uses as a catalyst support for hydrogenation of nitroaromatics. *ACS Appl. Mater. Interfaces* **2016**, *8*, 9881–9888.

[27] Wang, N.; Yang, G.; Wang, H. X.; Yan, C. Z.; Sun, R.; Wong, C. P. A universal method for large-yield and high-concentration exfoliation of two-dimensional hexagonal boron nitride nanosheets. *Mater. Today* **2019**, *27*, 33–42.

[28] Chen, Y.; Kang, Q.; Jiang, P. K.; Huang, X. Y. Rapid, high-efficient and scalable exfoliation of high-quality boron nitride nanosheets and their application in lithium-sulfur batteries. *Nano Res.* **2021**, *14*, 2424–2431.

[29] Yan, Q. W.; Dai, W.; Gao, J. Y.; Tan, X.; Lv, L.; Ying, J. F.; Lu, X. X.; Lu, J. B.; Yao, Y. G.; Wei, Q. P. et al. Ultrahigh-aspect-ratio boron nitride nanosheets leading to superhigh in-plane thermal conductivity of foldable heat spreader. *ACS Nano* **2021**, *15*, 6489–6498.

[30] Chen, Y.; Liu, Y. J.; Liu, X. Y.; Li, P. L.; Li, Z.; Jiang, P. K.; Huang, X. Y. On-demand preparation of boron nitride nanosheets for functional nanocomposites. *Small Methods* **2024**, *8*, 2301386.

[31] Wang, H. G.; Lu, R. J.; Li, L.; Liang, C.; Yan, J.; Liang, R.; Sun, G. X.; Jiang, L.; Cheng, Q. F. Strong, tough, and thermally conductive nacre-inspired boron nitride nanosheet/epoxy layered nanocomposites. *Nano Res.* **2024**, *17*, 820–828.

[32] Navik, R.; Tan, H. J.; Zhang, H.; Shi, L. Y.; Li, J.; Zhao, Y. P. High-throughput and scalable exfoliation of large-sized ultrathin 2D materials by ball-milling in supercritical carbon dioxide. *Small Methods* **2024**, *8*, 2301334.

[33] Wu, K.; Fang, J. C.; Ma, J. R.; Huang, R.; Chai, S. G.; Chen, F.; Fu, Q. Achieving a collapsible, strong, and highly thermally conductive film based on oriented functionalized boron nitride nanosheets and cellulose nanofiber. *ACS Appl. Mater. Interfaces* **2017**, *9*, 30035–30045.

[34] Teng, C.; Su, L. Y.; Chen, J. X.; Wang, J. F. Flexible, thermally conductive layered composite films from massively exfoliated boron nitride nanosheets. *Compos. Part A: Appl. Sci. Manuf.* **2019**, *124*, 105498.

[35] Huang, J. Z.; E, S. F.; Li, J. Y.; Jia, F. F.; Ma, Q.; Hua, L.; Lu, Z. Q. Ball-milling exfoliation of hexagonal boron nitride in viscous hydroxyethyl cellulose for producing nanosheet films as thermal interface materials. *ACS Appl. Nano Mater.* **2021**, *4*, 13167–13175.

[36] Zhang, J.; Lu, C.; He, J. X. Simple and efficient synthesis of flexible boron nitride nanosheets/aramid nanofiber composite films with high thermal conductivity and strength. *J. Alloys Compd.* **2024**, *978*, 173536.

[37] Lin, Y.; Williams, T. V.; Xu, T. B.; Cao, W.; Elsayed-Ali, H. E.; Connell, J. W. Aqueous dispersions of few-layered and monolayered hexagonal boron nitride nanosheets from sonication-assisted

hydrolysis: Critical role of water. *J. Phys. Chem. C* **2011**, *115*, 2679–2685.
[38] Li, Q. Y.; Ye, J.; Xiong, J.; Abidi, N. Structures and high fluorescence of novel nanocomposites of sodium carboxymethyl cellulose/Tb(III) prepared at different pHs. *Polym. Compos.* **2017**, *38*, E498–E507.
[39] Yang, L. S.; Wang, D. S.; Liu, M. S.; Liu, H. M.; Tan, J. Y.; Wang, Z. Y.; Zhou, H. Y.; Yu, Q. M.; Wang, J. Y.; Lin, J. H. et al. Glue-assisted grinding exfoliation of large-size 2D materials for insulating thermal conduction and large-current-density hydrogen evolution. *Mater. Today* **2021**, *51*, 145–154.
[40] Li, X. M.; Qiu, H.; Liu, X. F.; Yin, J.; Guo, W. L. Wettability of supported monolayer hexagonal boron nitride in air. *Adv. Funct. Mater.* **2017**, *27*, 1603181.
[41] Zhuang, Z. T.; Chen, H. W.; Li, C. Robust pristine MXene films with superhigh electromagnetic interference shielding effectiveness via spatially confined evaporation. *ACS Nano* **2023**, *17*, 10628–10636.
[42] Tu, H.; Xie, K.; Lin, X. H.; Zhang, R. Q.; Chen, F.; Fu, Q.; Duan, B.; Zhang, L. N. Superior strength and highly thermoconductive cellulose/ boron nitride film by stretch-induced alignment. *J. Mater. Chem. A* **2021**, *9*, 10304–10315.
[43] Wu, Y. P.; Xue, Y.; Qin, S.; Liu, D.; Wang, X. B.; Hu, X.; Li, J. L.; Wang, X. G.; Bando, Y.; Golberg, D. et al. BN nanosheet/polymer films with highly anisotropic thermal conductivity for thermal management applications. *ACS Appl. Mater. Interfaces* **2017**, *9*, 43163–43170.
[44] Wang, J. M.; Wu, Y. P.; Xue, Y.; Liu, D.; Wang, X. B.; Hu, X.; Bando, Y.; Lei, W. W. Super-compatible functional boron nitride nanosheets/polymer films with excellent mechanical properties and ultra-high thermal conductivity for thermal management. *J. Mater. Chem. C* **2018**, *6*, 1363–1369.
[45] Yoo, S. C.; Park, Y. K.; Park, C.; Ryu, H.; Hong, S. H. Biomimetic artificial nacre: Boron nitride nanosheets/gelatin nanocomposites for biomedical applications. *Adv. Funct. Mater.* **2018**, *28*, 1805948.
[46] Ma, T. B.; Zhao, Y. S.; Ruan, K. P.; Liu, X. R.; Zhang, J. L.; Guo, Y. Q.; Yang, X. T.; Kong, J.; Gu, J. W. Highly thermal conductivities, excellent mechanical robustness and flexibility, and outstanding thermal stabilities of aramid nanofiber composite papers with nacre-mimetic layered structures. *ACS Appl. Mater. Interfaces* **2020**, *12*, 1677–1686.
[47] Wu, K.; Wang, J. M.; Liu, D. Y.; Lei, C. X.; Liu, D.; Lei, W. W.; Fu, Q. Highly thermoconductive, thermostable, and super-flexible film by engineering 1D rigid rod-like aramid nanofiber/2D boron nitride nanosheets. *Adv. Mater.* **2020**, *32*, 1906939.
[48] An, L. L.; Gu, R.; Zhong, B.; Wang, J. L.; Zhang, J. Y.; Yu, Y. L. Quasi-isotropically thermal conductive, highly transparent, insulating and super-flexible polymer films achieved by cross linked 2D hexagonal boron nitride nanosheets. *Small* **2021**, *17*, 2101409.
[49] Wu, K.; Zhang, Y. Z.; Gong, F.; Liu, D. Y.; Lei, C. X.; Fu, Q. Highly thermo-conductive but electrically insulating filament via a volume-confinement self-assembled strategy for thermoelectric wearables. *Chem. Eng. J.* **2021**, *421*, 127764.
[50] Li, Y. W.; Huang, T. Q.; Chen, M.; Wu, L. M. Simultaneous exfoliation and functionalization of large-sized boron nitride nanosheets for enhanced thermal conductivity of polymer composite film. *Chem. Eng. J.* **2022**, *442*, 136237.
[51] Li, L. H.; Li, M. H.; Zhang, Z. H.; Qin, Y.; Shui, X. X.; Xia, J. C.; Xiong, S. Y.; Wang, B.; Zhang, Z. B.; Wei, X. Z. et al. Robust composite film with high thermal conductivity and excellent mechanical properties by constructing a long-range ordered sandwich structure. *J. Mater. Chem. A* **2022**, *10*, 9922–9931.
[52] Zhao, L. H.; Wang, L.; Jin, Y. F.; Ren, J. W.; Wang, Z.; Jia, L. C. Simultaneously improved thermal conductivity and mechanical properties of boron nitride nanosheets/aramid nanofiber films by constructing multilayer gradient structure. *Compos. Part B: Eng.* **2022**, *229*, 109454.
[53] Song, N.; Wang, P.; Jin, L. Y.; Zhang, F.; Wang, Z. F.; Ding, P. Tunable oriented cellulose/BNNSs films designed for high-performance thermal management. *Chem. Eng. J.* **2022**, *437*, 135404.
[54] Xu, L. S.; Zhan, K.; Ding, S. Y.; Zhu, J. Y.; Liu, M. S.; Fan, W. R.; Duan, P.; Luo, K.; Ding, B. F.; Liu, B. L. et al. A malleable composite dough with well-dispersed and high-content boron nitride nanosheets. *ACS Nano* **2023**, *17*, 4886–4895.
[55] Wang, L. D.; Wang, B.; Wang, Z. Q.; Huang, J. J.; Li, K. W.; Liu, S. P.; Lu, J. H.; Han, Z. P.; Gao, Y.; Cai, G. F. et al. Superior strong and tough nacre-inspired materials by interlayer entanglement. *Nano Lett.* **2023**, *23*, 3352–3361.
[56] Han, Y. X.; Ruan, K. P.; Gu, J. W. Multifunctional thermally conductive composite films based on fungal tree-like heterostructured silver nanowires@boron nitride nanosheets and aramid nanofibers. *Angew. Chem., Int. Ed.* **2023**, *62*, e202216093.
[57] Yu, L.; Gao, T. T.; Mi, R. Y.; Huang, J.; Kong, W. Q.; Liu, D. P.; Liang, Z. Q.; Ye, D. D.; Chen, C. J. 3D-printed mechanically strong and extreme environment adaptable boron nitride/cellulose nanofluidic macrofibers. *Nano Res.* **2023**, *16*, 7609–7617.
[58] Du, Y.; Zhen, F. Z.; Ding, S. Y.; Zhong, Y. N.; Li, P. X.; Zhan, K.; Dong, M. H.; Guo, Z. J.; Fan, W. R.; Hin, O. E. et al. Anisotropic heat transfer in a fibrous membrane with hierarchically assembled 2D materials. *ACS Appl. Mater. Interfaces* **2024**, *16*, 65366–65377.
[59] Wu, R. X.; Song, X. D.; Ji, Y.; Wu, H.; Guo, S. Y.; Qiu, J. H. *In-situ* exfoliation of hexagonal boron nitride during the forced flow of highly elastic polylactide to fabricate electrospun fibrous film with high thermal conductivity and low dielectric loss. *Compos. Sci. Technol.* **2024**, *251*, 110573.
[60] Liu, M. X.; Ma, R. Y.; Wang, Z. X.; Li, Z. Y.; Song, G. L.; Lin, J.; Li, X. Y.; Xu, L.; Yan, D. X.; Jia, L. C. et al. Scalable assembly of micron boron nitride into high-temperature-resistant insulating papers with superior thermal conductivity. *Mater. Horiz.* **2025**, *12*, 4349–4362.
[61] Wu, W. L.; Zhan, T. Z.; Wang, P.; Li, Z. X.; Li, B.; Meng, L.; Niu, Z. F.; Ma, S. J.; Chen, H. R.; Zhang, J. et al. Fusing-smashing exfoliation for high-aspect-ratio hexagonal boron nitride nanosheets available to highly-thermoconductive polymeric composites. *Chem. Eng. J.* **2025**, *510*, 161451.
[62] Qi, C. S.; Luo, C.; Tao, Y.; Lv, W.; Zhang, C.; Deng, Y. Q.; Li, H.; Han, J. W.; Ling, G. W.; Yang, Q. H. Capillary shrinkage of graphene oxide hydrogels. *Sci. China Mater.* **2020**, *63*, 1870–1877.
[63] Zeng, X. L.; Ye, L.; Yu, S. H.; Li, H.; Sun, R.; Xu, J. B.; Wong, C. P. Artificial nacre-like papers based on noncovalent functionalized boron nitride nanosheets with excellent mechanical and thermally conductive properties. *Nanoscale* **2015**, *7*, 6774–6781.
[64] Wu, K.; Liao, P.; Du, R. N.; Zhang, Q.; Chen, F.; Fu, Q. Preparation of a thermally conductive biodegradable cellulose nanofiber/hydroxylated boron nitride nanosheet film: The critical role of edge-hydroxylation. *J. Mater. Chem. A* **2018**, *6*, 11863–11873.
[65] Su, L. Y.; Ma, X. Y.; Zhou, J. L.; Liu, X. C.; Du, F. L.; Teng, C. Large-scale preparation of high-performance boron nitride/aramid nanofiber dielectric composites. *Nano Res.* **2022**, *15*, 8648–8655.
[66] Li, X.; Wu, B.; Lv, Y.; Xia, R.; Qian, J. S. Effect of regulating the interfacial structure of multiple non-covalent bonding on improving thermal management capability. *J. Mater. Chem. A* **2024**, *12*, 864–875.